

# Breaking the “Redshift Deadlock” – II: The redshift distribution for the submillimetre population of galaxies

Itziar Aretxaga<sup>1</sup>, David H. Hughes<sup>1</sup>, Edward L. Chapin<sup>1</sup>, Enrique Gaztañaga<sup>2,1</sup>, James S. Dunlop<sup>3</sup>

<sup>1</sup>*Instituto Nacional de Astrofísica, Óptica y Electrónica (INAOE), Aptdo. Postal 51 y 216, 72000 Puebla, Mexico*

<sup>2</sup>*IEEC/CSIC, Edifici Nexus-201, c/ Gran Capitán 2-4, 08034 Barcelona, Spain*

<sup>3</sup>*Institute for Astronomy, University of Edinburgh, Blackford Hill, Edinburgh, EH9 3HJ, UK*

2 December 2024

## ABSTRACT

Ground-based sub-mm (SCUBA) and mm-wavelength (MAMBO) blank-field surveys have identified more than 100 sources, the majority of which are believed to be dusty optically-obscured starburst galaxies. Colours derived from various combinations of FIR, submillimetre, millimetre, and radio fluxes provide the only currently available means to determine the redshift distribution of this new galaxy population.

In this paper we apply our Monte-Carlo photometric-redshift technique, introduced in paper I (Hughes et al. 2002), to the multi-wavelength data available for 77 galaxies selected at 850 $\mu$ m and 1.25 mm. Unlike earlier redshift estimates, we calculate a probability distribution for the redshift of each galaxy. These estimates include a detailed treatment of the observational errors and uncertainties in the evolutionary model. The cumulative redshift distribution of the sub-mm galaxy population that we present in this paper, based on 47 galaxies with a S/N > 3.5 at 850 $\mu$ m found in wide-area SCUBA surveys, is asymmetric, and broader than those published elsewhere, with a significant high- $z$  tail. Approximately 40 to 90 per cent of the sub-mm population is expected to have redshifts in the interval  $2 \leq z \leq 4$ . Whilst this result is completely consistent with earlier estimates for the sub-mm galaxy population, we also show that the colours of many ( $\lesssim 50$  per cent) individual sub-mm sources are consistent with those of starburst galaxies that lie at extreme redshifts,  $z > 4$ . Spectroscopic confirmation of the redshifts, through the detection of rest-frame FIR-mm wavelength molecular transition-lines, will ultimately calibrate the accuracy of this technique. We use the redshift probability distribution of HDF850.1 to illustrate the ability of the method to guide the choice of possible frequency tunings on the broad-band spectroscopic receivers that equip the large aperture single-dish mm and cm-wavelength telescopes.

**Key words:** submillimetre, millimetre, cosmology, galaxy evolution, star-formation

## 1 INTRODUCTION

The lack of redshift information is one of the outstanding problems in understanding the nature of the presumed high-redshift galaxies identified in blank-field sub-mm and mm wavelength surveys.

In paper I of this series (Hughes et al. 2002) we described Monte Carlo simulations of 250–500 $\mu$ m surveys from the balloon-borne telescope BLAST (Devlin et al. 2001) and the SPIRE instrument on the Herschel satellite, and ground-based 850 $\mu$ m surveys with SCUBA. These simulations included a detailed treatment of the observational and evolutionary model-dependent errors. The sub-mm colours of

galaxies derived from these mock catalogues demonstrated that it will be possible to derive photometric redshifts, with a conservative r.m.s. accuracy of  $\Delta z \sim \pm 0.5$ , for thousands of optically-obscured galaxies. Thus we can look forward to breaking the redshift deadlock which, at the moment, prevents a reliable estimate of the evolutionary history of a population that contributes a significant fraction to the sub-mm background: 50–60% at 1–2 mJy (Hughes et al. 1998, Smail et al. 2002).

In this second paper we apply the same Monte Carlo photometric-redshift technique to the existing FIR–radio multi-wavelength data of 77 sources first identified in blank-field 850 $\mu$ m (SCUBA) and 1.2 mm (MAMBO) surveys. We

calculate the redshift probability distributions of the individual sub-mm and mm galaxies, taking into account observational and model-dependent uncertainties, and thus provide an accurate description of the cumulative redshift distribution of the blank-field sub-mm galaxy population.

The structure of the paper is as follows: section 2 gives a brief description of the Monte Carlo simulations, the method to derive photometric redshifts from the radio–sub-mm–FIR colours of galaxies drawn from the mock catalogues, and the caveats and advantages of this technique over other redshift indicators; section 3 presents individual redshift probability distributions for blank-field sub-mm galaxies. In addition, we include a brief discussion of the photometric redshifts for radio and FIR-selected galaxies subsequently detected at  $850\mu\text{m}$ . Furthermore, we determine the accuracy of our method through the comparison of the photometric redshifts for those 6 sub-mm sources that have rest-frame optical spectroscopic redshifts. Finally, in section 3 we present the cumulative redshift distribution of the blank-field sub-mm population. Section 4 discusses the likelihood of a radio detection of previously detected blank-field sub-mm sources, based only on the known dispersion of the  $850\mu\text{m}/1.4\text{ GHz}$  colour in starburst galaxies, radio-quiet AGN and ULIRGs, which are believed to be representative of the high- $z$  sub-mm galaxy population. Section 5 describes how the determination of redshift probability distributions for individual sub-mm galaxies is motivating the efforts to provide spectroscopic confirmation of the redshifts at mm and cm wavelengths. Ultimately, these spectroscopic redshifts will accurately calibrate the photometric redshifts derived from rest-frame FIR–radio-wavelength data. Appendix A contains the complete catalogue of spectral energy distributions (SEDs) and redshift distributions derived in this paper.

## 2 PHOTOMETRIC REDSHIFT ESTIMATION TECHNIQUE

The Monte Carlo simulations described in this paper produce the redshift probability distribution for an individual galaxy. The advantage of this technique, compared to the popular maximum-likelihood methods, is that it provides more information than an estimate of the first and second moments of the redshift distributions. A detailed description of the technique can be found in paper I; we only offer a summary here. Hereafter we will refer to a galaxy detected in a SCUBA or MAMBO survey as a *sub-mm* galaxy, and a sub-mm galaxy generated in the Monte Carlo simulations as a *mock* galaxy.

We choose an evolutionary model for the  $60\mu\text{m}$  luminosity function that fits the observed  $850\mu\text{m}$  number-counts. Under this model, and assuming a sub-mm survey of  $\sim 10\text{ deg}^2$ , we generate a catalogue of  $60\mu\text{m}$  luminosities and redshifts. Randomly selected template SEDs are drawn from a library of local starbursts, ULIRGs and AGN, to provide FIR–radio fluxes, and hence colours, for this mock catalogue. The fluxes of the mock galaxies include both photometric and calibration errors, consistent with the quality of the observational data for the sub-mm galaxy. We reject from the catalogue those mock galaxies that do not respect the detection thresholds and upper-limits of the particular sub-mm galaxy under analysis. In this paper the redshift probability

distribution of a sub-mm galaxy is calculated as the normalized distribution of the redshifts of the mock galaxies in the reduced catalogue, weighted by the likelihood of identifying the colours and fluxes of each mock galaxy with those of the sub-mm galaxy in question. Thus, we also take into account as much prior information on the sub-mm galaxy population (and their uncertainties) as possible. For example, we consider uncertainties in the sub-mm galaxy number counts, their favoured evolutionary models, the luminosity function of dusty galaxies, lensing by a foreground magnifying cluster, etc. In the case that the sub-mm galaxy is identified as a lensed source, then the mock catalogue is also amplified by the appropriate factor, allowing intrinsically fainter objects to be introduced into the reduced catalogue, using the same observational measurement errors.

We adopt a flat,  $\Lambda$ -dominated cosmological model ( $H_0 = 67\text{ km s}^{-1}\text{ Mpc}^{-1}$ ,  $\Omega_M = 0.3$ ,  $\Omega_\Lambda = 0.7$ ). To quantify the sensitivity of the individual redshift distributions on the assumed evolutionary history of the sub-mm galaxy population, we consider four different models that are able to reproduce the observed  $850\mu\text{m}$  number-counts within the uncertainties. We will refer to them by the following codes:

**z10:** luminosity evolution of the  $60\mu\text{m}$  luminosity function  $\Phi[L, z = 0]$  (Saunders et al. 1990) as  $(1 + z)^{3.2}$  for  $0 < z < 2.2$ . Constant evolution is imposed between  $z = 2.2 - 10$ . No galaxies beyond  $z = 10$ ,  $\Phi[L, z > 10] = 0$ .

**z10L13:** same evolutionary description as in z10, but imposing a luminosity cut-off above  $10^{13}L_\odot$ .

**z6:** luminosity evolution of  $\Phi[L, 0]$  as  $(1 + z)^3$  for  $0 < z < 2.3$ . Constant evolution is imposed between  $z = 2.3 - 6$ .  $\Phi[L, z > 6] = 0$ .

**z6L13:** same evolutionary description as in z6, but imposing a luminosity cut-off above  $10^{13}L_\odot$ .

The SEDs assigned in the Monte Carlo are drawn from an extended library compared to paper I, and contains 20 starbursts, ULIRGs and AGN with luminosities in the range  $9.0 \lesssim \log L_{\text{FIR}}/L_\odot \lesssim 12.3$  (M 82, NGC 3227, NGC 2992, NGC 4151, NGC 7469, NGC 7771, NGC 1614, I Zw 1, Mkn 231, Arp 220, Mkn 273, NGC 6240, UGC 5101, IRAS 10214+4724, IRAS 05189–2524, IRAS 08572+3915, IRAS 15250+3609, IRAS 12112+0305, IRAS 14348–1447 and Cloverleaf). The SEDs are fitted by physically-motivated functional relationships (Chapin et al. 2002). Our SED library is composed of galaxies that have been either extensively mapped at FIR–radio wavelengths, or of galaxies that are sufficiently distant that single-beam photometric observations measure the total flux. This selection has the important consequence of reducing any dispersion in the SEDs due to aperture effects.

Half of the galaxies in the SED library used in the derivation of photometric redshifts in this paper are in common with those considered by Yun & Carilli (2002), hereafter YC02. The temperature range covered by our sample of galaxies (25 – 65K, median 41K) is broader than that of YC02 due to the increased fraction of cooler sources, and is, for the same reason, colder than those of well-studied ULIRGs (46 – 77K, median 60K, Klaas et al. 2001). Despite the similar temperatures of our sample to late-type galaxies selected at  $60\mu\text{m}$  (25 – 55K, median 35K), drawn from the SLUGS catalogue of Dunne et al. (2000), the shapes of the SEDs in our library differ significantly from the local galax-

ies in the SLUGS. This illustrates an important point: it is the shapes of the SEDs, and not the derived dust temperatures, that influence the estimated photometric redshifts. Given the limited FIR–sub-mm data, there is a degeneracy between the dust temperatures, grain emissivity index ( $\beta$ ), source-size ( $\Omega$ ) and optical depth ( $\tau_\nu$ ). This makes it possible to fit a single observed SED with a broad range of temperature, by tuning the choice of  $\beta$ ,  $\Omega$  and  $\tau_\nu$  (e.g. Hughes et al. 1993).

It remains unclear whether the lower-luminosity, local galaxies in the SLUGS are closely related to the blank-field SCUBA population which have rest-frame FIR luminosities  $> 10^{12} L_\odot$ , provided the sub-mm galaxies lie at  $z > 1$ . The claim that cold SEDs match the number-counts in hydrodynamical cosmological simulations (e.g. Fardal et al. 2002) should not be a basis for favouring cold SEDs, since a different evolutionary model with warmer SEDs can fit the counts equally well (e.g. paper I).

The strongest caveat in any photometric redshift analysis is the validity of the assumption that the SED templates of local starbursts, ULIRGs and AGN are good analogs of the high-redshift sub-mm galaxy population. It is not until future rest-frame FIR–sub-mm observations from sensitive balloon-borne or satellite experiments (paper I) accurately measure the variety of SEDs present in the sub-mm galaxy population, that it will be possible to improve the error estimates presented in this paper.

The technique adopted in this paper differs philosophically from those developed in other photometric-redshift studies. Our redshift estimates do not rely on the match of the observed data to a single template SED, and our errors are not drawn from the departure of other local SEDs from the adopted standard template, which has become the common practice (Carilli & Yun 1999, 2000, hereafter referred to as CY99, CY00; Gear et al. 2000; YC02). Instead, we allow the test galaxies to be matched against the whole variety of template SEDs that can be detected at any given redshift. This point should be emphasized, since although we assign our template SEDs at random, not all SED shapes (scaled to the same FIR luminosity) are detected with equal probability at any given redshift and wavelength. The redshift distributions derived in this paper are often asymmetric, and broader than those inferred from the single SED template analysis. Despite the efforts of some authors to include realistic error-bars in their single-template estimates, we consider these to have been underestimated: error bars derived from 68% of the galaxies in a template catalogue, is not equivalent to the 68% dispersion in the fluxes that the whole catalogue can create, since some of the outliers contribute very significantly to the departures from the mean.

Our redshift estimation method also has the advantage of including a common-sense evaluation of whether a source at a given redshift is simultaneously consistent with the observed colours and fluxes. The probability of generating a certain luminosity at a certain redshift (*i.e.* flux) is introduced by the luminosity function and the evolutionary model adopted. As shown below, when sub-mm galaxies with detections at more than two wavelengths are considered, the results are insensitive to the differences in the evolutionary models adopted to generate the mock catalogue. The inclusion of a reasonable evolutionary model, however,

allows plausible colour-based redshift solutions to be excluded.

### 3 MONTE CARLO BASED PHOTOMETRIC REDSHIFTS

The available data-set for the sub-mm population of galaxies is usually restricted to a low-S/N detection at  $850\mu\text{m}$  and an upper-limit at  $450\mu\text{m}$  (from SCUBA surveys), or a 1.2 mm detection (from MAMBO surveys), with, perhaps, follow-up radio observations at 1.4, 5 or 8.6 GHz. Although a number of the SCUBA surveys have been conducted in fields previously observed by the Infrared Space Observatory (ISO) with the ISOPHOT camera at 170 and  $90\mu\text{m}$ , *e.g.* HDF (Hughes et al. 1998; Borys et al. 2002), ELAIS N2 (Scott et al. 2002; Fox et al. 2002), and the Lockman Hole (Scott et al. 2002; Fox et al. 2002), the ISO measurements are generally too shallow to provide any additional constraint on the photometric redshifts.

The method described in section 2 produces mock-catalogues that replicate the sensitivities and calibration accuracies of the original surveys in which each sub-mm galaxy was detected. The colours and fluxes of the mock galaxies provide diagnostic diagrams to illustrate the derivation of the most probable redshift: colour-colour-redshift ( $C - C - z$ ) diagrams, when more than 3-band detections are available; colour-flux-redshift ( $C - f - z$ ) diagrams, when just two bands are available; and flux-redshift ( $f - z$ ) diagrams; when just one band detection is available. From these diagrams we derive the corresponding redshift probability distribution ( $P - z$ ) for each sub-mm galaxy. The distributions for a selection of sub-mm galaxies considered in this paper are shown in Appendix A.

#### 3.1 Specific examples: LH850.1 and BCR11

LH850.1 is the brightest  $850\mu\text{m}$  source identified in the wide-area UK 8 mJy SCUBA survey of the Lockman Hole (Scott et al. 2002), and has one of the most complete FIR–radio SEDs (Lutz et al. 2001). BCR11, named after source 11 in the sub-mm catalogue of Barger, Cowie & Richards (2000), is a low S/N, but nonetheless representative,  $850\mu\text{m}$  source detected in a follow-up SCUBA photometry survey of the micro-Jansky 1.4 GHz radio sources in the Hubble Deep Field (Richards 2000).

Even though BCR11 was not first identified in a blank-field sub-mm survey, and hence is not included in the combined redshift distribution of the sub-mm galaxy population, it provides a useful source to discuss. The sub-mm photometry observations of BCR11 at the position of a known radio source (Richards 2000) guarantees that we have the correct association of a radio and sub-mm source, and hence the correct SED to analyse. BCR11 allows us to confidently derive the photometric redshift and accuracy that we can expect from only the 1.4 GHz/ $850\mu\text{m}$  colour, which is commonly used to measure redshifts of blank-field sub-mm galaxies with follow-up radio observations (CY99, CY00).

Figs. 1,2,3, respectively, show the  $C - C - z$  and  $P - z$  distributions for the multi-wavelength data of LH850.1, and the comparison of the observed SED and template SEDs (redshifted to the mode of the  $P - z$  distribution). Figs. 4,5,6

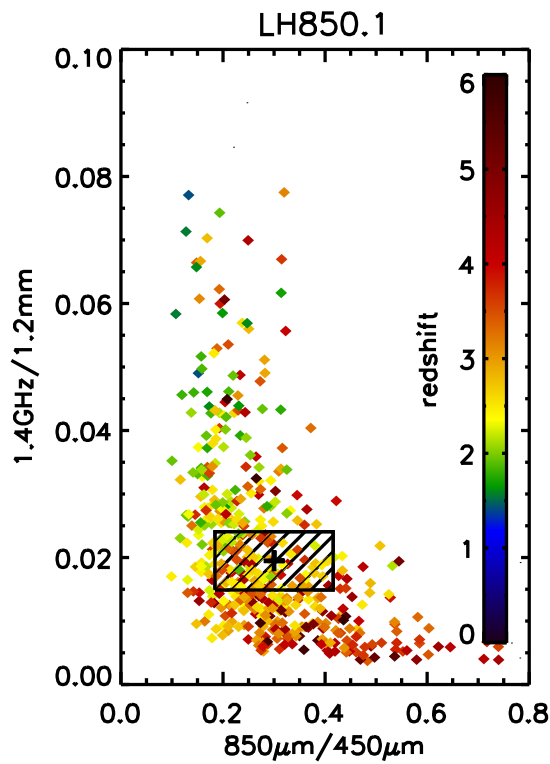


**Figure 1.** Colour-colour-redshift ( $C - C - z$ ) plot for LH850.1 (Lutz et al. 2001, Scott et al. 2002). The flux ratios of the mock galaxies, generated under the evolutionary model z6 (section 2), are represented as diamonds, and their redshifts are coded in colour according to the scale shown to the right of the panel. The black cross represents the measured colours of LH850.1, and the dashed box shows the  $1\sigma$  uncertainty in each colour.

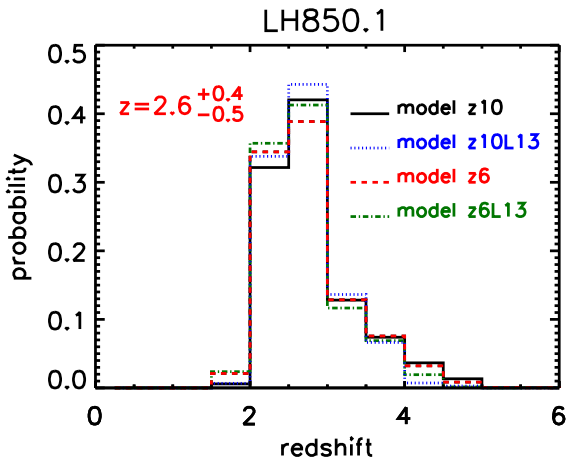


**Figure 2.** Redshift probability distributions of LH850.1. The four estimates (lines of different style and color) correspond to the four evolutionary models introduced in section 2. The mode of the redshift distribution and the 68% confidence level interval for model z6 are shown.

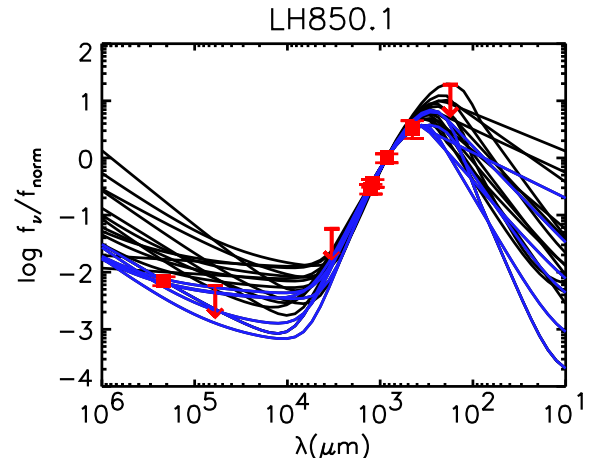


**Figure 3.** The observed SED of LH850.1 normalised to the flux density at  $850\mu\text{m}$  is shown as squares and arrows. The arrows indicate  $3\sigma$  upper limits. The squares denote detection at a level  $\geq 3\sigma$ , with  $1\sigma$  error bars. The template SEDs (lines) are redshifted to the mode of the redshift probability distribution,  $z = 2.6$ . The template SEDs compatible within  $3\sigma$  error bars with the SED of LH850.1 are displayed in blue.

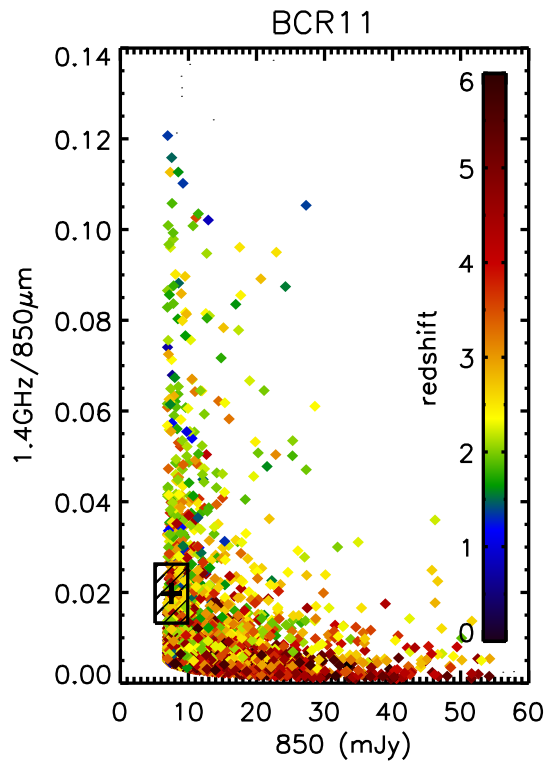


**Figure 4.** Colour-flux-redshift ( $C - f - z$ ) plot for BCR11 (Barger et al. 2000). The description of the symbols is as in Fig. 1

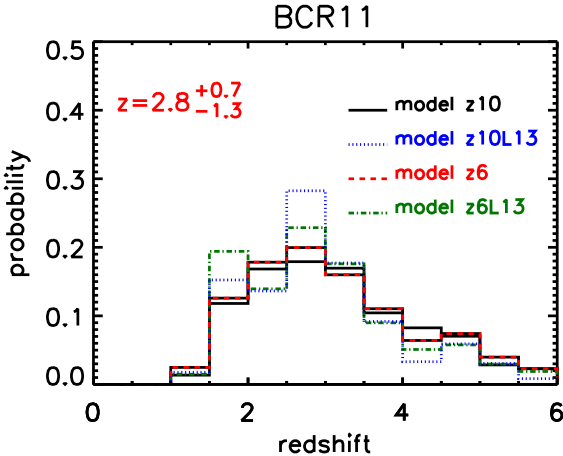


**Figure 5.** Redshift probability distributions for BCR11. The description of the plot is as in Fig. 2

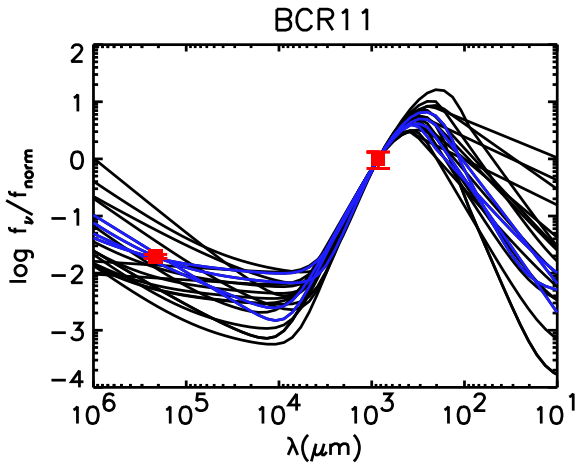


**Figure 6.** Comparison of the observed SED of BCR11 with those of template galaxies. The description of the plot is as in Fig. 3. Note that the selection of SEDs to represent BCR11 is different from that in LH850.1.

show the same distributions for BCR11. In both examples (Figs. 2 and 5) the redshift distribution is insensitive to the details of the evolutionary model used to compute the mock catalogues.

The comparison of LH850.1 and BCR11 demonstrates the improved redshift accuracy that, in general, one can expect for those sources with the greatest combination of deep multi-wavelength data. In the case of BCR11, it also illustrates the difficulty of constraining redshifts with observations at 1.4 GHz and 850  $\mu$ m only. The redshift probability distributions of both sources have very similar modes ( $z = 2.6 - 2.8$ ), yet there remains 50% and 23% probabilities that BCR11 has a redshift  $> 3$  and  $> 4$  respectively. The corresponding probabilities for LH850.1 are 26% and 6% respectively. This improvement in constraint on the photometric redshift is extremely important if it is to be used to determine the tuning of any broad-band mm–cm spectrograph,

in an attempt to detect redshifted molecular CO-lines. This is discussed further in section 5.

With only limited ground-based data available, the higher frequency radio observations at  $\sim 5 - 15$  GHz and deep 450  $\mu$ m observations, including upper-limits, are essential and provide the additional diagnostic power to discriminate between redshifts (e.g. LH850.1).

### 3.2 Individual redshift distributions

Before we calculate the cumulative redshift-distribution for the 850  $\mu$ m sources detected in the wide-area ( $> 200$  sq. arcmin) blank-field SCUBA surveys, which include the Lockman Hole and ELAIS N2 regions (Scott et al. 2002; Fox et al. 2002), and the CUDSS fields (Lilly et al. 1999; Eales et al. 2000; Webb et al. 2002), it is instructive to discuss some of the typical redshift distributions that can be derived from data of different quality (i.e. sensitivity and wavelength coverage) for individual sources.

Therefore, we first consider the typical redshift distributions of the above sub-mm sources, and complement these with the redshift distributions of sub-mm sources detected in various lensing-cluster surveys (Smail et al. 1997; Smail et al. 1999; Bertoldi et al. 2000; Chapman et al. 2002). We also consider radio, FIR and UV-selected objects with follow-up sub-mm data (Barger et al. 2000; Scott et al. 2000; Chapman et al. 2000), and two bright sub-mm sources with extensive multi-wavelength observations, HDF850.1 (Hughes et al. 1998; Downes et al. 1999; Dunlop et al. 2002), and HR10 (Dey et al. 1999).

Tables 1, 2, and 3 summarize the photometric redshifts of all the above sources: the modes of their redshift distributions, 68% and 90% confidence intervals, and other relevant information. Appendix A contains the  $C - C - z$ ,  $C - f - z$ ,  $P - z$  diagrams and SEDs of the galaxies listed in Tables 1 and 2, and a selection of those listed in Table 3.

The SEDs in Appendix A (Figs. A1) show that when we have the most complete multi-wavelength data-set (rest-frame radio–sub-mm–FIR, including upper limits) then photometric redshifts can be constrained to a 68% confidence band of width  $\Delta z \sim \pm 0.5$ . Those sub-mm galaxies for which just two detections, and perhaps some shallow upper-limits are available, do much worse, with accuracies at a 68% confidence level of width  $\Delta z \gtrsim \pm 1$  (Figs. A2). A merit of the Monte Carlo photometric-redshift method is that it can determine redshift probability distributions even in the case that the galaxies have just been detected in one band (Fig. A3), the result being very flat redshift distributions, that are highly dependent on the assumed evolutionary model. This is especially important because most of the sub-mm sources in the blank-field surveys belong to this category.

Often, the well constrained distributions are asymmetric, skewed towards lower redshifts with a high-redshift tail (e.g. LH850.1, N2850.2, HR10, ... in Fig. A1). This is a natural consequence of the ability of the data (particularly with a deep 450  $\mu$ m detection or upper limit,  $< 30$  mJy) to strongly reject the possibility of sub-mm galaxies lying at  $z \lesssim 2$ , whilst the same observational data cannot reject the possibility that the sub-mm galaxies lie at a much higher redshift,  $z \gg 3$ . Examples of the power with which the 450  $\mu$ m detections or upper-limits can reject  $z \lesssim 2$  can be seen in the

SEDS of LH850.1 and HDF850.1 (Fig. A1), respectively. On the other hand, the bright ISOPHOT detections at  $170\mu\text{m}$  ( $> 120\text{mJy}$ ) make a strong case that the sources lie at  $z \lesssim 2$ , for example N1–063 (Fig. A1) and N1–008 (Fig. A2), whilst the ISOPHOT non-detections are too shallow to offer any additional constraints on the SEDs of the majority of the sub-mm population (e.g. LH850.1, HDF850.1 in Fig. A1)

It is also possible to obtain a bimodal redshift probability distribution for some galaxies (e.g. SMMJ00266+1708 in Fig. A1, BCR33 in Fig. A2), an effect created by two or more template SEDs reproducing the same observed colours at very different redshifts.

The figures in appendix A show the insensitivity of the  $1.4\text{GHz}/850\mu\text{m}$  ratio to redshift when the sources are at  $z \gtrsim 2$  (a point also made by CY99, CY00). The redshift distributions in these cases are usually shallow, with long high-redshift tails (e.g. BCR11, BCR13, MMJ154127+6615, in Fig. A2), although exceptions also occur (SMMJ16403+4644 in Fig. 2A). The distributions are even broader in the cases when only a sub-mm detection and a radio upper-limit are available (Fig. A3).

A quick browse through Appendix A illustrates the variety of template SEDs that reproduce the colours of an individual sub-mm galaxy, which lends support to the use of a template library in the derivation of the photometric redshifts. A few sub-mm sources, however, still cannot be reproduced at any redshift with the template SEDs available (e.g. CUDSS3.8, SMMJ16403+46437). A possible explanation for this problem is the contribution of AGN emission to the radio-fluxes at a level not included in the SEDs of the template library, or a mis-identification of a sub-mm galaxy with a nearby radio-source (see also section 4). Other sub-mm galaxies have only a small representation of analogs among the mock galaxies (e.g. N1-008, CUDSS3.8, SMMJ14009+0252). This latter point is illustrated by the rarity of mock galaxies in the corresponding  $C - C - z$  or  $C - f - z$  diagrams.

### 3.2.1 Accuracy of the photometric-redshift method

Fig. 7 shows the comparison of photometric and spectroscopic redshifts for 6 sub-mm galaxies: in order of increasing spectroscopic redshift, CUDSS14.18, SMMJ02399-0134, HR10, SMMJ14011+0252, SMMJ02399-0136, and W-MM11.

The two galaxies which depart most from the  $z_{\text{phot}} = z_{\text{spec}}$  line are SMMJ02399-0134 and W-MM11. The first has a photometric redshift calculated only on the basis of its  $1.4\text{GHz}/850\mu\text{m}$  colour (Fig. A2), and the latter on a  $850\mu\text{m}$  detection with a  $450\mu\text{m}$  upper limit (Fig. A3). These two objects illustrate the large confidence intervals that have to be considered when the redshifts are derived from a single colour. Specifically, SMMJ02399-0134 illustrates the uncertainties attached to the large dispersion of  $1.4\text{GHz}/850\mu\text{m}$  colours implied from a local sample of galaxies. The agreement between spectroscopic and photometric redshifts for the remaining four galaxies (with more than one colour available) is remarkably good. The asymmetry of the error bars of the two lowest redshift sources (CUDSS14.18 and HR10) is a reflection of the skewness of their respective  $P - z$  (Figs. A1, A2). These sources illustrate the importance of obtain-

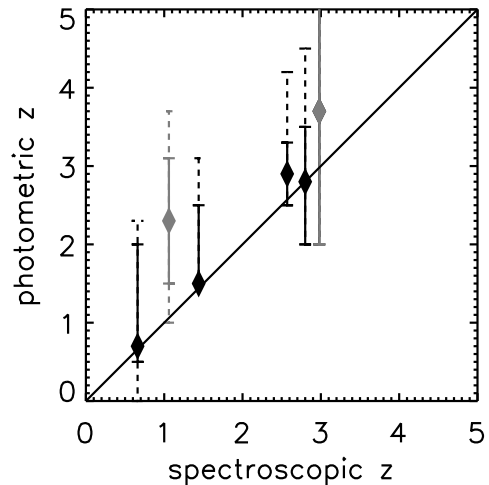


**Figure 7.** Comparison of the photometric-redshift estimates and the true redshifts of sub-mm sources with optical/IR spectroscopy. The diamonds represent the modes of the redshift distributions. The solid and dashed error bars represent 68% and 90% confidence intervals, respectively. Sources represented in black (in increasing redshift: CUDSS14.18, HR10, SMMJ14011+0252, and SMMJ02399-0136) have photometric redshifts derived from a combination of colours, and are the most precise. Sources represented in grey (in increasing redshift: SMMJ02399-0134, and W-MM11) have photometric redshifts derived from only one colour (or limit), and have shallow probability distributions, still compatible with their spectroscopic redshifts. Note that the asymmetry of the error-bars is a reflection of the asymmetry of the redshift probability distributions, which in cases (CUDSS14.18 and HR10) are significantly skewed.

ing the description of the whole redshift distribution instead of relying on measurements of the first moment.

A larger sample of spectroscopic redshifts is essential to assess the statistical significance of the goodness of this technique, and the accuracy of the error bars we derive (which, in part, are the result of the scatter in the shapes of the template SEDs).

### 3.2.2 Notes on individual sources

**LH850.1:** Other redshift estimates are  $2.95 \pm 0.08^{1.49}$  based on the  $1.4\text{GHz}/850\mu\text{m}$  spectral index technique; and  $2.72 \pm 0.37$  based on a  $\chi^2$  minimization with one template SED (YC02). Our own estimate  $z = 2.6 \pm 0.4$  is consistent with these measurements.

**HDF850.1:** Other redshift estimates are  $> 2.6$ , based on the  $1.4\text{GHz}/850\mu\text{m}$  spectral index technique; and  $4.11 \pm 0.51$  based on a  $\chi^2$  minimization with one template SED (YC02). Our own estimate  $z = 4.1 \pm 0.6$  is in good agreement with these measurements, and is unaffected by the inclusion of the possible lensing amplification experienced by this source ( $A \approx 2$ , Dunlop et al. 2002).

**CUDSS14.1:** Other published redshift estimates are  $2.01 \pm 0.71^{1.10}$ , based on the  $1.4\text{GHz}/850\mu\text{m}$  spectral index technique; and  $2.06 \pm 0.31$  based on a  $\chi^2$  minimization with

**Table 1.** Sub-mm sources detected in three or more passbands at a  $\geq 3\sigma$  level, except where otherwise stated. Columns 1–7 give the name of the source, the survey in which it was first detected, the references for the SED data, the mode of photometric-redshift distribution, the 68% and 90% confidence intervals for the photometric redshift, and notes for each object. The references are coded as follows: (1) Lutz et al. 2001, (2) Scott et al. 2002, (3) Ciliegi et al. 1999, (4) Downes et al. 2001, (5) Dunlop et al. 2002; (6) Eales et al. 2000, (7) Smail et al. 1999, (8) Frayer et al. 2000, (9) Ivison et al. 1998, (10) Ivison et al. 2000, (11) Dey et al. 1999, (12) Scott et al. 2000. The  $A$  in the notes denotes the amplification factor reported in the literature for the lensed sources.

object	survey	ref.	$z$	68% CL	90% CL	notes
LH850.1	UK 8mJy	1	2.6	(2.1 – 3.0)	(2.0 – 3.7)	
N2850.1	UK 8mJy	2,3	2.8	(2.0 – 3.1)	(2.0 – 3.9)	
N2850.2	UK 8mJy	2,3	2.3	(2.0 – 2.9)	(2.0 – 3.7)	
HDF850.1	UK HDF	4,5	4.1	(3.5 – 4.7)	(3.0 – 5.2)	
CUDSS14.1	Canada-UK Deep	6	3.8	(2.8 – 4.5)	(2.5 – 5.6)	
SMMJ00266+1708	SCUBA Lensed 1	7,8	3.9	(2.5 – 5.0)	(2.0 – 5.8)	$A = 1.6$
SMMJ02399–0136	SCUBA Lensed 1	8,9	3.9	(3.0 – 4.8)	(2.5 – 5.0)	$z_{\text{spec}} = 2.8, A = 2.4, 3.4\text{cm too low?}$
				2.8	(2.0 – 3.5)	disregarding the 3.4cm upper limit
SMMJ09429+4658	SCUBA Lensed 1	7	2.6	(2.5 – 3.3)	(2.5 – 4.2)	$A = 1.$
SMMJ14009+0252	SCUBA Lensed 1	10	3.4	(2.6 – 4.5)	(2.0 – 5.0)	$A = 1.5$
SMMJ14011+0252	SCUBA Lensed 1	8	2.9	(2.5 – 3.5)	(2.5 – 4.0)	$z_{\text{spec}} = 2.57, A = 3.$
HR10	K-band selection	11	1.5	(1.5 – 2.4)	(1.5 – 3.1)	$z_{\text{spec}} = 1.44$
N1-063	ISO-FIRBACK	12	1.2	(0.5 – 1.6)	(0.5 – 2.0)	> $2\sigma$ detections taken into account

**Table 2.** Sub-mm sources detected in two pass-bands at  $\geq 3\sigma$  level. The columns are identical to those described in Table 1. The reference codes are as follows: (1) Scott et al. 2002, (2) Ciliegi et al. 1999, (3) Barger et al. 2000, (4) Eales et al. 2000, (5) Webb et al. 2002, (6) Smail et al. 1999, (7) Chapman et al. 2002, (8) Bertoldi et al. 2000, (9) Dannerbauer et al. 2002, (10) Scott et al. 2001.

object	survey	ref.	$z$	68% CL	90% CL	notes
LH850.8	UK 8 mJy	1,2	3.6	(2.5 – 4.6)	(2.0 – 5.0)	
LH850.12	UK 8 mJy	1,2	2.3	(1.5 – 3.1)	(1.5 – 4.0)	
N2850.4	UK 8 mJy	1,2	3.3	(2.5 – 4.1)	(2.0 – 4.5)	
BCR7	Hawaii HDF	3	2.7	(1.5 – 3.5)	(1.5 – 4.8)	
BCR11	Hawaii HDF	3	2.7	(1.5 – 3.7)	(1.5 – 4.9)	
BCR13	Hawaii HDF	3	3.3	(2.0 – 4.4)	(1.5 – 5.7)	
BCR33	Hawaii HDF	3	3.2	(1.9 – 4.0)	(1.5 – 5.5)	
BCR49	Hawaii HDF	3	2.4	(2.0 – 3.8)	(2.0 – 4.5)	
CUDSS14.3	Canada-UK Deep	4	3.3	(2.0 – 4.2)	(2.0 – 5.3)	
CUDSS14.9	Canada-UK Deep	4	2.7	(2.0 – 3.6)	(1.5 – 4.2)	
CUDSS14.18	Canada-UK Deep	4	0.7	(0.4 – 2.0)	(0.0 – 2.3)	$z_{\text{spec}} = 0.66$
CUDSS3.1	Canada-UK Deep	5	1.7	(1.5 – 2.5)	(1.0 – 2.4)	
CUDSS3.8	Canada-UK Deep	5	2.2	(1.5 – 2.8)	(1.0 – 3.0)	high 1.4GHz, AGN?
CUDSS3.9	Canada-UK Deep	5	1.1	(0.7 – 1.5)	(0.5 – 1.6)	
CUDSS3.10	Canada-UK Deep	5	2.7	(1.6 – 3.5)	(1.5 – 4.5)	
CUDSS3.15	Canada-UK Deep	5	2.4	(1.5 – 3.3)	(1.5 – 4.0)	
SMMJ02399–0134	SCUBA Lensed 1	6	2.3	(1.5 – 3.1)	(1.0 – 3.7)	$A = 2.5$
SMMJ10236+0412	SCUBA Lensed 2	7	2.4	(1.5 – 3.2)	(1.5 – 4.0)	$A = 3.2$
SMMJ10237+0410	SCUBA Lensed 2	7	2.0	(1.5 – 3.2)	(1.0 – 3.6)	$A = 3.7$
SMMJ16403+4644	SCUBA Lensed 2	7	2.2	(1.4 – 3.0)	(0.7 – 3.1)	$A = 3.0$
SMMJ16403+46440	SCUBA Lensed 2	7	2.7	(2.0 – 3.5)	(2.0 – 4.0)	$A = 3.6$
SMMJ16403+46437	SCUBA Lensed 2	7	2.2	(1.5 – 3.1)	(1.0 – 3.5)	$A = 3.2, 1.4\text{GHz high, AGN?}$
MMJ154127+6615	MAMBO Lensed	8	3.5	(2.5 – 4.8)	(2.0 – 6.2)	$A = 1$
MMJ154127+6616	MAMBO Lensed	8	2.8	(2.5 – 5.0)	(2.0 – 6.7)	$A = 1$
MMJ120546–0741.5	MAMBO	9	3.8	(3.0 – 6.0)	(3.0 – 8.4)	
MMJ120539–0745.4	MAMBO	9	2.7	(2.5 – 5.1)	(2.0 – 6.2)	
N1–008	ISO-FIRBACK	10	0.0	(0.0 – 0.4)	(0.0 – 0.5)	

**Table 3.** Sub-mm sources detected at  $850\mu\text{m}$  or  $1.2\text{mm}$  at a  $\geq 3.5\sigma$  level, and undetected at any other wavelength. The columns are identical to those described in Table 1. The reference codes are as follows: (1) Scott et al. 2002, (2) Eales et al. 2000, (3) Webb et al. 2002, (4) Smail et al. 1999, (5) Chapman et al. 2002, (6) Dannerbauer et al. 2002.

object	survey	ref.	$z$	68% CL	90% CL	notes
LH850.2	UK 8mJy	1	4.0	(3.0 – 6.9)	(2.5 – 8.5)	
LH850.3	UK 8mJy	1	4.5	(2.9 – 7.0)	(2.5 – 8.5)	
LH850.4	UK 8mJy	1	4.0	(2.9 – 7.0)	(2.5 – 8.5)	
LH850.5	UK 8mJy	1	4.8	(3.0 – 7.0)	(2.5 – 8.6)	
LH850.6	UK 8mJy	1	5.2	(3.0 – 7.0)	(2.5 – 8.6)	
LH850.7	UK 8mJy	1	4.2	(2.5 – 6.5)	(2.0 – 8.4)	
LH850.9	UK 8mJy	1	4.7	(2.6 – 6.5)	(2.5 – 8.7)	
LH850.10	UK 8mJy	1	4.0	(2.5 – 6.5)	(2.0 – 8.2)	
LH850.11	UK 8mJy	1	4.4	(3.0 – 6.8)	(2.5 – 8.6)	
LH850.13	UK 8mJy	1	3.9	(2.0 – 6.2)	(2.0 – 8.4)	
N2850.3	UK 8mJy	1	4.5	(3.0 – 6.9)	(2.5 – 8.5)	
N2850.5	UK 8mJy	1	4.2	(3.0 – 7.0)	(2.5 – 8.5)	
N2850.6	UK 8mJy	1	3.9	(2.5 – 6.4)	(2.0 – 8.3)	
N2850.7	UK 8mJy	1	4.7	(2.9 – 7.0)	(2.0 – 8.5)	
N2850.8	UK 8mJy	1	4.1	(2.2 – 6.5)	(2.0 – 8.5)	
N2850.9	UK 8mJy	1	4.0	(2.2 – 6.5)	(2.0 – 8.4)	
N2850.10	UK 8mJy	1	4.0	(2.2 – 6.5)	(2.0 – 8.6)	
N2850.11	UK 8mJy	1	4.3	(2.4 – 6.5)	(2.0 – 8.4)	
CUDSS14.2	Canada-UK Deep	2	4.7	(3.0 – 7.0)	(2.5 – 8.8)	
CUDSS14.4	Canada-UK Deep	2	4.6	(3.5 – 7.5)	(2.5 – 8.8)	
CUDSS14.5	Canada-UK Deep	2	4.8	(3.5 – 7.5)	(3.0 – 9.0)	
CUDSS14.6	Canada-UK Deep	2	5.0	(3.5 – 7.7)	(2.5 – 8.8)	
CUDSS14.8	Canada-UK Deep	2	4.8	(3.0 – 7.2)	(2.5 – 9.0)	
CUDSS14.10	Canada-UK Deep	2	4.5	(2.8 – 7.0)	(2.5 – 9.0)	
CUDSS3.2	Canada-UK Deep	3	3.5	(2.0 – 6.3)	(2.0 – 8.7)	
CUDSS3.3	Canada-UK Deep	3	3.4	(2.2 – 6.5)	(2.0 – 8.5)	
CUDSS3.4	Canada-UK Deep	3	3.8	(2.0 – 6.2)	(2.0 – 8.6)	
CUDSS3.5	Canada-UK Deep	3	3.8	(2.0 – 6.3)	(2.0 – 8.7)	
CUDSS3.6	Canada-UK Deep	3	3.7	(2.0 – 6.3)	(2.0 – 8.7)	
CUDSS3.7	Canada-UK Deep	3	3.8	(2.4 – 6.5)	(2.0 – 8.5)	
CUDSS3.11	Canada-UK Deep	3	4.2	(2.2 – 6.5)	(2.0 – 8.5)	
CUDSS3.12	Canada-UK Deep	3	3.3	(2.0 – 6.3)	(2.0 – 8.6)	
CUDSS3.13	Canada-UK Deep	3	3.8	(2.0 – 6.3)	(2.0 – 8.5)	
CUDSS3.16	Canada-UK Deep	3	4.1	(2.0 – 6.5)	(2.0 – 8.5)	
SMMJ02400–0134	SCUBA Lensed 1	4	5.3	(3.5 – 7.6)	(3.0 – 9.1)	$A > 1.9$ (2.5?)
SMMJ04431+0210 (N4)	SCUBA Lensed 1	4	4.3	(2.9 – 7.0)	(2.5 – 8.8)	$A > 1.?$
SMMJ22471–0206	SCUBA Lensed 1	4	4.7	(3.0 – 7.2)	(2.8 – 8.8)	$A > 1.9$ (2.5?)
SMMJ04541–0302	SCUBA Lensed 2	5	4.5	(2.8 – 7.0)	(2.5 – 8.9)	$A = 2.6$
SMMJ04542–0301	SCUBA Lensed 2	5	4.7	(2.8 – 7.0)	(2.5 – 8.5)	$A = 4.5$
SMMJ04543+0256	SCUBA Lensed 2	5	4.5	(2.5 – 6.8)	(2.0 – 8.5)	$A = 3.1$
SMMJ04543+0257	SCUBA Lensed 2	5	4.2	(3.0 – 7.0)	(2.0 – 8.2)	$A = 3.4$
SMMJ10237+0412	SCUBA Lensed 2	5	4.5	(2.5 – 6.9)	(2.0 – 8.7)	$A = 3.5$
SMMJ14573+2220	SCUBA Lensed 2	5	4.7	(2.5 – 6.8)	(2.0 – 8.5)	$A = 2.8$
SMMJ17223+3207	SCUBA Lensed 2	5	4.5	(2.5 – 6.7)	(2.0 – 8.4)	$A = 2.8$
MMJ120517–0743.1	MAMBO	6	7.0	(5.0 – 9.1)	(4.5 – 10.0)	
W-MM11	Lyman-break galaxy	7	3.7	(2.0 – 6.2)	(2.0 – 8.6)	$z_{\text{spec}} = 2.98$

one template SED (YC02). Both these estimates are in the low-redshift tail of our redshift distribution, which at a 68% significance level places this object at  $z = 3.8 \pm 1.0$ .

**CUDSS14.18:** The inclusion of the 450 and  $850\mu\text{m}$  fluxes as detections at  $2.3$  and  $2.8\sigma$  (instead of upper limits) gives a similar distribution to the one shown in Figure A2. Our redshift estimate places this object at  $z = 0.7 \pm 0.2$  with a 68% confidence level, in good agreement with its true spectroscopic redshift,  $z_{\text{spec}} = 0.66$ . Other redshift estimates are  $1.12 \pm 0.53$ , based on the  $1.4\text{GHz}/850\mu\text{m}$  spectral index tech-

nique; and  $1.11 \pm 0.21$  based on a  $\chi^2$  minimization with one template SED (YC02).

**SMMJ00266+1708:** Other redshift estimates are  $3.49 \pm 2.03$  based on the  $1.4\text{GHz}/850\mu\text{m}$  spectral index technique; and  $3.50 \pm 0.45$  based on a  $\chi^2$  minimization with one template SED (YC02). Our estimate  $z = 3.9 \pm 1.4$  is consistent with these measurements. The redshift distribution is bimodal, due to the range of SEDs used in the redshift estimation technique, and hence broader than that of YC02

**SMMJ02399–0136:** The complete SED reported in Frayer et al. (2000), Ivison et al. (1998) is inconsistent with the SEDs of our template library at any redshift. The 3.4cm upper limit is too low to support the extrapolation of the synchrotron tail to high frequencies. A high-frequency synchrotron cut-off at these frequencies has been noted in other nearby starbursts and ULIRGs (*e.g.* M 82, Hughes, Gear & Robson 1990). Since these sharp spectral features are not taken into account in the fitting of the radio spectrum, we disregard for the moment the 3.4cm upper limit of SMMJ02399–0136. The resulting redshift estimation  $z = 2.8 \pm 0.8$  is in good agreement with the true redshift of SMMJ02399–0136:  $z = 2.80$ . Other redshift estimates are  $1.65 \pm 0.80$  based on the 1.4GHz/850 $\mu$ m spectral index technique; and  $2.83 \pm 0.38$  based on a  $\chi^2$  minimization with one template SED (YC02).

**SMMJ09429+4658 (H5):** Other redshift estimates are  $\geq 3.6$  based on the 1.4GHz/850 $\mu$ m spectral index technique; and  $3.86 \pm 0.49$  based on a  $\chi^2$  minimization with one template SED (YC02). Our estimates actually place this source at a slightly lower redshift  $z = 2.6 \pm 0.7$ . Given the sub-mm detection, the low flux density at 1.4 GHz excludes almost all of the template SEDs in our library.

**SMMJ14009+0252:** Other redshift estimates are  $1.27 \pm 0.54$  based on the 1.4GHz/850 $\mu$ m spectral index technique; and  $1.30 \pm 0.23$  based on a  $\chi^2$  minimization with one template SED (YC02). However large discrepancies ( $\sim 3\sigma$ ) exist between the template SED of YC02 and the observed 450 $\mu$ m and 1.4GHz fluxes, suggesting the fit will have a high reduced- $\chi^2$ , and that their errors (inferred for good matches) might be under-estimated. The flattening of the spectrum at 450 $\mu$ m, relative to the Raleigh-Jeans tail defined by the 850 $\mu$ m and 1.35mm fluxes, supports a higher redshift estimate. Our own fit indicates that this object has a redshift  $z = 3.4 \pm 1.1$ , while redshifts between  $z = 1 - 1.5$  have a probability of only 1.3%. The 1.4 GHz flux (529 $\mu$ Jy) is high for a sub-mm source, and is barely compatible with our library of templates at  $z = 3.4$  (see the scarce coverage of the colour-colour-redshift plot in Appendix A). A redshift estimate that disregards the 1.4GHz flux detection ( $z = 3.3 \pm 0.8$ ), however, remains consistent with our initial higher-redshift measurement.

**SMMJ14011+0252:** Other redshift estimates are  $2.53 \pm 0.82$  based on the 1.4GHz/850 $\mu$ m spectral index technique; and  $2.73 \pm 0.37$  based on a  $\chi^2$  minimization with one template SED (YC02). Our own estimate is  $z = 2.9 \pm 0.4$  in good agreement with these estimates, and with the spectroscopic redshift of the optical counterpart  $z_{\text{spec}} = 2.57$ .

**HR10:** Other redshift estimates are  $1.49 \pm 0.75$  based on the 1.4GHz/850 $\mu$ m spectral index technique; and  $1.75 \pm 0.28$  based on a  $\chi^2$  minimization with one template SED (YC02). Our own estimate  $z = 1.5 \pm 0.9$  is in good agreement with their measurements, and with the true spectroscopic redshift of this source  $z_{\text{spec}} = 1.44$ .

**N1–063:** The inclusion of  $\sim 2.4$  and  $2.8\sigma$  measurements at 170 and 450 $\mu$ m as detections allows the determination of its redshift distribution to a higher degree of accuracy, than if just the 850 $\mu$ m detection had been taken into account (see Fig. A3).

**SMMJ02399–0134:** Other redshift estimates are  $1.17 \pm 0.45$  based on the 1.4GHz/850 $\mu$ m spectral index technique; and  $0.93 \pm 0.19$  based on a  $\chi^2$  minimization with one

template SED (YC02). The spectroscopic redshift of this source ( $z_{\text{spec}} = 1.06$ ) is inconsistent with our best estimate of the redshift, which within a 68% confidence interval places it at  $z = 2.3 \pm 0.8$ . There is a 10% integrated probability in the  $1.0 \leq z \leq 1.5$  interval of the redshift distribution.

**SMMJ16403+46437:** The detection at 1.4GHz (593 $\mu$ Jy) is high when compared with the 850 $\mu$ m level, and there is not an acceptable correspondence with any of the SEDs in our template library. This, plausibly, might be a misidentification or a radio-quiet AGN, with enhanced radio luminosity compared to the rest-frame FIR luminosity.

**SMMJ16403+46440:** Treating the 1.35mm observation as a detection ( $2.2\sigma$ ) provides no additional constraint and gives a similar redshift distribution to the one shown in Figure A2.

### 3.3 Cumulative redshift distribution of the sub-mm galaxy population

It is straightforward to calculate the cumulative redshift distribution for the sub-mm galaxy population as the coaddition of the individual probability distributions. It should be noted that the calculation carried out in this paper has the advantage of including the whole redshift probability distribution of each individual galaxy, and not just the mean values of the distributions. We have included in this calculation of the cumulative distribution only those sub-mm sources identified in wide-area blank-field surveys (UK 8mJy survey and the CUDSS) at a  $\geq 3.5\sigma$  level: 47 sources. We do not include sub-mm galaxies identified in surveys carried out towards lensing clusters, or targeted observations of other populations of galaxies (radio, ISO, Lyman-break galaxies or extremely red objects), or catalogs that have not been fully published (MAMBO surveys), since they can distort and bias the characteristic redshift distribution of the sub-mm galaxy population.

The majority of sources in complete flux-limited sub-mm samples, such as the UK 8mJy and CUDSS surveys, have a single 850 $\mu$ m detection with one, or more, additional upper-limits at other wavelengths: 34/47 sources detected ( $> 3.5\sigma$ ) at 850 $\mu$ m belong to this category. Since the redshift distributions of these sources are the most dependent on the priors used, we will consider an additional extreme evolutionary model to those introduced in section 2. The model z4L13 provides pure luminosity evolution,  $(1+z)^{3.2}$ , of the 60 $\mu$ m luminosity between  $0 < z < 3$ , and constant evolution between  $z = 3 - 4$ . No galaxies beyond  $z = 4$ , or with luminosities larger than  $10^{13} L_{\odot}$  are allowed. This model under-produces the number-counts at  $S_{850\mu\text{m}} < 1 \text{ mJy}$  for our library of SEDs, and the luminosity cut-off is mandatory in order not to over-produce the number-counts above 8 mJy. This extreme model, which is consistent with the source-counts at  $S_{850\mu\text{m}} > 1 \text{ mJy}$  helps demonstrate the obvious strong dependence of the cumulative redshift distribution on the evolutionary model, when the observational data provide poor constraints on redshift.

Fig. 8 shows the cumulative distribution and the combined redshift distribution of the 6 galaxies in the UK 8mJy survey with “well-constrained” redshift distributions, *i.e.*, those derived from SEDs which contain at least 2-band detections (objects in Tables 1 and 2). This figure indicates that 85 per cent of the sub-mm galaxies have redshifts in

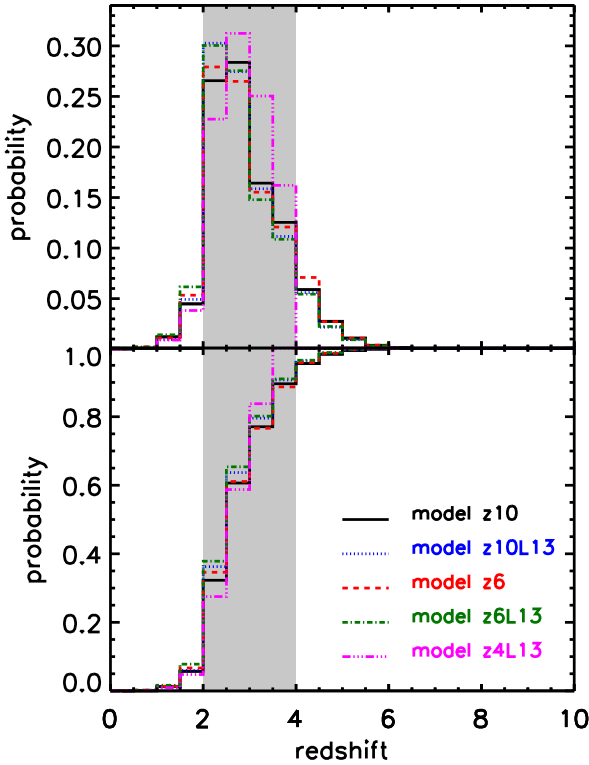
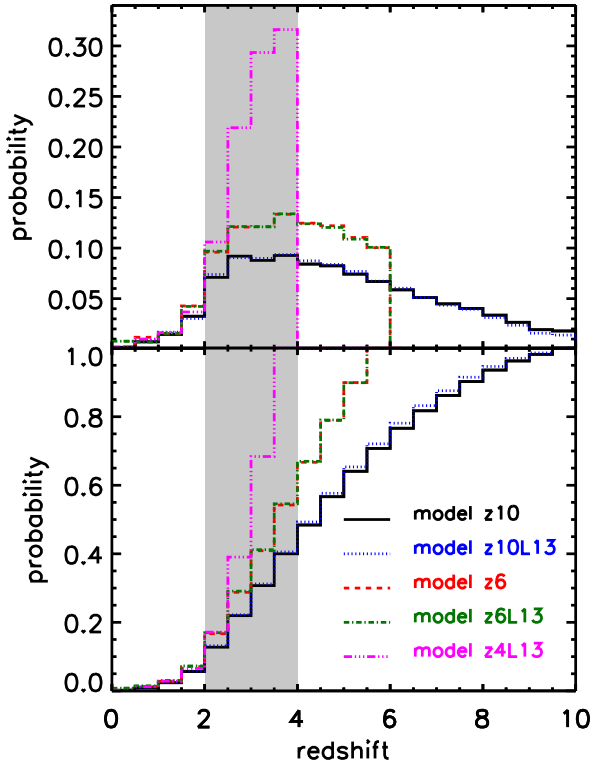


**Figure 8.** Combined redshift distribution for the population of sub-mm galaxies in the 8mJy survey with well-constrained redshift distributions (the 6 galaxies contained in Tables 1 & 2). The different lines represent different evolutionary models assumed for the sub-mm galaxy population (section 2). *Upper panel:* discrete bin probabilities. *Lower panel:* cumulative distribution.

the range  $2 \lesssim z \lesssim 4$ . The results are consistent with the expectation that sub-mm galaxies detected in the SCUBA (and also MAMBO) surveys represent a high- $z$  population (see Dunlop 2001 for a review).

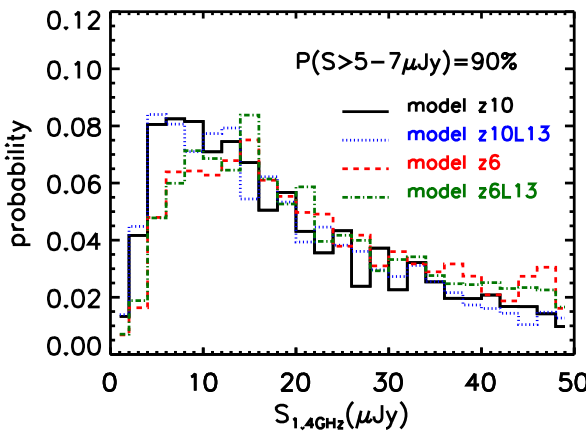
The “well-constrained” sources in the CUDSS sample (7 sources) appear to have a significantly different lower redshift distribution, with 40 per cent of the galaxies at  $z \lesssim 2$  and approximately 50 per cent of the galaxies at  $2 \lesssim z \lesssim 4$ . The high redshift tail of the CUDSS sample is similar to that shown by the 8mJy survey with 10 per cent probability at  $z > 4$ . The galaxies responsible for the low-redshift difference are CUDSS3.1 and 3.9, both with relatively high  $450\mu\text{m}$  flux densities  $S_{450\mu\text{m}} \geq 77$  mJy, compared with the 30–40 mJy detection levels for the UK 8mJy survey sources. Taking the data for the CUDSS sample at face-value suggests that it includes an over-density of low- $z$  galaxies at  $z \lesssim 2$ , compared to the galaxies in the UK 8mJy survey. This discrepancy, however, can most easily be explained by a difference in the flux-calibration of the  $450\mu\text{m}$  data in the two surveys.

Fig. 9 shows the cumulative redshift distributions of the sub-mm galaxy population for the 47 galaxies in the 8mJy and CUDSS surveys detected at a  $\geq 3.5\sigma$  level. This extended sample includes the 34 sub-mm galaxies with a single



**Figure 9.** Combined redshift distribution for the population of all 47 sub-mm galaxies detected in wide-area surveys at  $850\mu\text{m}$  ( $> 3.5\sigma$ ). The different lines represent different evolutionary models assumed for the sub-mm galaxy population (see text). Beware that the extended tail towards high-redshifts is due to sources for which just  $850\mu\text{m}$  are available. The upper limits in other bands do not usually constrain their redshifts between values 2 and 10, and hence their probability distributions are very flat in those regimes. *Upper panel:* discrete bin probabilities. *Lower panel:* cumulative distribution.

detection at  $850\mu\text{m}$  and one, or more, upper limits at other wavelengths (Table 3). The combined redshift distributions, for the different evolutionary models under consideration, imply that the majority of the sub-mm galaxies, approximately 50–90 per cent, lie between  $z = 2–4$ . The remainder of the galaxies,  $\sim 10$  per cent, lie at  $z < 2$ . Fig. 9 also shows that  $\lesssim 50$  per cent of the galaxies have colours that are consistent with  $z > 4$ . The distribution of the high-redshift tail is very sensitive to the choice of evolutionary model, since the individual redshift distributions for the 34 sources with only a single detection are necessarily very flat over the redshift range  $z \gtrsim 2$  (see Fig. A3). For these galaxies, the constraint on their redshift distributions comes mainly from the flux detected at  $850\mu\text{m}$  and the ability to reproduce it with the evolution of the luminosity function.



**Figure 10.** Distribution of fluxes at 1.4GHz corresponding to a population of galaxies discovered at  $850\mu\text{m}$ , at a level  $\geq 8\text{mJy}$ . Depending on the evolutionary model adopted, 90% of the sources would have a flux in excess of 5 to  $7\mu\text{Jy}$ , and hence in order to conduct a parallel 1.4GHz imaging follow-up program with 90% completeness, the  $1\sigma$  depth of the images should be 1.6 to  $2.3\mu\text{Jy}$ .

#### 4 THE LIKELIHOOD OF MIS-IDENTIFYING THE RADIO COUNTERPARTS OF HIGH- $z$ SUB-MM GALAXIES

The strength of the correlation between the FIR and radio luminosities in starburst galaxies (Helou et al. 1985, Condon 1992) has supported the expectation that *all* high- $z$  star forming sub-mm galaxies should also have a detectable radio-counterpart, provided the radio observations are deep enough.

Although originally encouraged by this assumption, the early VLA searches for radio emission associated with SCUBA and MAMBO sources have met with limited success. For example, the deep VLA surveys of the Hubble Deep Field reached noise levels of  $7.5\mu\text{Jy}$  at 1.4 GHz and  $1.6\mu\text{Jy}$  at 8.4 GHz (Richards et al. 1998, Richards 2000), yet both failed to achieve significant, or unambiguous detections of the sub-mm galaxies identified in one of the deepest SCUBA surveys (Hughes et al. 1998).

Shallower, larger-area VLA surveys of the ELAIS N2 field (Ciliegi et al. 1999) and Lockman Hole field (de Ruiter et al. 1997) necessarily have a higher noise limit ( $1\sigma > 26\mu\text{Jy}$  at 1.4 GHz). The lack of any significant correlation between the VLA sources and the sub-mm sources identified in wide-area SCUBA surveys of both fields (Scott et al. 2002; Fox et al. 2002) again indicates that the radio observations have failed to identify the counterparts of these bright blank-field sub-mm galaxies.

We disagree with the claims of previous authors (Fox et al. 2002) that high- $z$  sub-mm sources should be detected at flux densities of  $\sim 100\mu\text{Jy}$  at 1.4 GHz. In Fig.10 we demonstrate that the current radio observations have insufficient sensitivity. Future VLA surveys at 1.4 GHz must reach a  $3\sigma$  sensitivity of  $5-7\mu\text{Jy}$  if radio observations are to provide counterparts to 90% of the high- $z$  sub-mm galaxies with  $850\mu\text{m}$  flux densities  $\sim 8\text{mJy}$ , according to the redshift distribution assumed in the different evolutionary models. If we

consider only those sub-mm galaxies with  $S_{850\mu\text{m}} \sim 8\text{mJy}$  at  $2 < z < 4$ , then the 1.4 GHz radio surveys must reach a  $3\sigma$  sensitivity of  $\sim 12\mu\text{Jy}$  in order to detect 90% of the radio counterparts.

This potential for misidentifying the correct radio sources associated with blank-field sub-mm galaxies will inevitably lead to incorrect estimates of photometric redshifts if they are derived in part from the 1.4 GHz fluxes. In the calculation of the cumulative redshift distribution (section 3.3) we have treated all of the published associations of 1.4 GHz and  $850\mu\text{m}$  sources as the correct radio counterparts to the sub-mm galaxies.

Despite the rapid acceptance of the radio–sub-mm flux density ratio,  $\alpha_{345}^{1.4}$  (CY99, CY00), as the preferred method with which to estimate the redshift distribution of the sub-mm galaxy population, this diagnostic ratio loses its power to discriminate between photometric redshifts at  $z > 2$  (CY99, CY00). We have already demonstrated in paper I (Fig. 11) the detrimental effect of the large dispersion in radio–sub-mm colours of the local template galaxies on the accuracy of the derived photometric redshifts of the sub-mm blank field sources. Furthermore, the existing radio interferometers will remain limited in their ability to map the large areas  $\sim 1-40$  sq. deg. that will be surveyed by the next generation of sub-mm and FIR experiments (e.g. BLAST, Herschel, SIRTF) down to the necessary sensitivity levels ( $3\sigma \sim 5-12\mu\text{Jy}$  at 1.4GHz), making the use of  $\alpha_{1.4}^{345}$  an impractical measure of redshift.

This limitation of the radio–sub-mm technique prompted the design and construction of a Balloon-borne Large Aperture Submillimetre Telescope, BLAST (Devlin et al. 2001). The primary scientific goal of BLAST is to break the current “redshift deadlock” by providing photometric redshifts with sufficient accuracy, without the prior necessity for secure optical, IR or radio counterparts. BLAST will use rest-frame sub-mm and FIR colours to derive redshifts with an accuracy  $\Delta z \sim \pm 0.5$  for  $> 1000$  galaxies in the redshift range  $0 < z < 6$  detected in wide-area ( $> 0.5\text{ deg}^2$ ) surveys at 250, 350 and  $500\mu\text{m}$  (Hughes et al. 2002).

This redshift accuracy is sufficient to guide the choice of possible front-end spectrographs, and their receiver tunings, on large single-dish ground-based mm and cm telescopes (e.g. 100-m GBT–Green Bank Telescope and 50-m LMT–Large Millimetre Telescope) in the effort to detect redshifted CO emission-lines. We describe one application of this technique below.

#### 5 BROAD-BAND MM–CM SPECTROSCOPY

Until recently the brightest sub-mm source in the Hubble Deep Field, HDF850.1 (Hughes et al. 1998), has avoided the detection of its X-ray, optical, IR or radio counterpart, despite an accurate interferometric position at 236 GHz (Downes et al. 1999) and the unprecedented depth of the multi-wavelength HDF surveys (Williams et al. 1996; Thompson et al. 1999; Richards 1999; Hornschmeier et al. 2000). It is only after the accurate subtraction of the elliptical galaxy, 3–586, at  $z \sim 1$ , however, that a faint IR counterpart ( $K = 23.5$ ,  $H - K = 1.5$ ,  $I - K > 5.1$ ) to HDF850.1 has been discovered, and furthermore, a combined data-set from MERLIN and the VLA has detected coincident radio

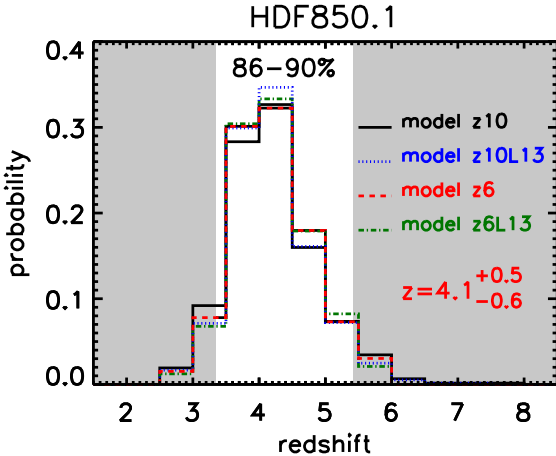


**Figure 11.** Redshift probability distributions for HDF850.1. The different line types and colours correspond to the different evolutionary models considered. The unshaded area corresponds to the observable K-band window (18.5 – 26.0 GHz), accessible with the 100m GBT. There is an 86–90% probability of detecting the J=1-0 CO-line in this window

emission with a flux density of  $16 \pm 4 \mu\text{Jy}$  at 1.4 GHz (Dunlop et al. 2002). A marginal  $3.3\sigma$  detection at 8.4 GHz (VLA 3651+1226, Richards, priv. comm.) is now also associated with HDF850.1.

The redshift probability distribution for HDF850.1, based on the multi-wavelength  $170\mu\text{m}$ –1.4 GHz data, indicates that  $z_{\text{phot}} = 4.1^{+0.5}$  with 68% confidence, and  $z_{\text{phot}} = 4.1 \pm 1.1$  with 90% confidence (Fig.11). This high photometric redshift supports the earlier decision to reject the elliptical galaxy 3–586, as the optical counterpart. Unfortunately the IR counterpart, HDF850.1K, is too faint to attempt IR spectroscopy with even the 10-m class of telescopes.

The most efficient means to determine the spectroscopic redshifts of optically-obscured sub-mm galaxies is the detection of millimetre and centimetre wavelength molecular lines using large single-dish telescopes (e.g. GBT or LMT) with broad-band receivers. In this way, it is possible to eliminate the necessity for an optical/IR counterpart, or a position accurate to  $< 3 \text{ arcsec}$ . For example, given the accuracy of the photometric redshift for HDF850.1, and taking all of the uncertainties discussed in section 2 into account, we demonstrate in Fig.11 that the J=1-0 CO line in HDF850.1 has a 86–90% probability of detection in the K-band receiver (18.0–26.5 GHz) on the GBT.

## 6 CONCLUSIONS

We have derived meaningful photometric-redshift probability distributions for individual sub-mm galaxies using Monte Carlo simulations that take into account a range of measurement errors and model-dependent uncertainties. From the individual redshift probability distributions, we have measured the cumulative redshift distribution for the sub-mm population of galaxies identified in blank field surveys. We find that the multi-wavelength FIR–radio data for 47 sub-

mm galaxies detected ( $> 3.5\sigma$ ) at  $850\mu\text{m}$  are consistent with  $\sim 50$ –90% of the population lying at redshifts  $z = 2$ –4, with only a small fraction,  $\sim 10\%$  of the population at  $z < 2$ . We also show that up to 50% of the galaxies have colours that are consistent with  $z > 4$ . The possibility that the sub-mm galaxy population contains a significant fraction undergoing a major burst of star formation at early epochs has important consequences for models of galaxy formation and evolution.

Shorter-wavelength sub-mm data (250 –  $500\mu\text{m}$ ) from a future balloon-borne experiment, BLAST, will provide strong additional constraints ( $\Delta z \sim \pm 0.5$ ) on the redshift distribution of all the SCUBA and MAMBO galaxies at  $z > 2$ . A photometric-redshift accuracy of  $\pm 0.5$  for an individual galaxy will be sufficient to provide robust statistical measurements of the redshift distribution of the entire population, the global history of dust-obscured star formation and the clustering properties of sub-mm galaxies.

We have argued that the large dispersion in the radio to sub-mm SEDs (or  $850\mu\text{m}$ /1.4GHz colour) of the template galaxies naturally translates into an imprecise measure of the photometric redshift, and that radio observations cannot be used efficiently to measure the individual redshifts of thousands of galaxies detected in future wide-area sub-mm surveys.

We have an on-going programme to conduct centimetre-wavelength observations of CO J=1-0 molecular line transitions in high- $z$  sub-mm galaxies on the 100-m GBT. The observations, however, first require an accurate photometric-redshift probability distribution to guide the choice of receiver and tuning parameters. We illustrate the power of our photometric-redshift technique with the example of HDF850.1, one of the best-studied sub-mm galaxies (Hughes et al. 1998; Downes et al. 1999; Dunlop et al. 2002).

Within the next few years, the combination of ground-based, balloon-borne and satellite experiments will provide accurately calibrated rest-frame sub-mm–FIR data for a significant population of sub-mm galaxies. The centimetre and millimetre wavelength spectroscopic redshift confirmation of their photometric redshifts will calibrate the method outlined in this paper. Thus we can finally look forward to breaking the “redshift deadlock” that currently prevents an accurate understanding of the nature of the optically-obscured sub-mm galaxy population and their evolutionary history.

## 7 ACKNOWLEDGMENTS

This work has been partly supported by CONACYT grants 32180-E and 32143-E.

## REFERENCES

- Barger A.J., Cowie, L.L, Richards, E.A., 2000, *A.J.*, 119, 2092
- Bertoldi F. et al., 2000, *A&A*, 360, 92.
- Borys, C, Chapman S.C, Halpern M., Scott D., 2002, *MNRAS*, 330, 63.
- Carilli C.L. & Yun M.S., 1999, *Ap.J.*, 513, L13 (*CY99*)
- Carilli C.L. & Yun M.S., 2000, *Ap.J.*, 530, 618 (*CY00*)
- Chapin E. et al, 2002, *MNRAS*, in preparation.
- Chapman S.C. et al. 2000, *MNRAS*, 319, 318.

Chapman S.C., Scott D., Borys C., & Fahlman G.G., 2002, MNRAS, 330, 92.

Ciliegi P. et al., 1999, MNRAS, 302, 222

Condon J.J., 1992, ARAA, 30, 575

Dannerbauer H. et al., 2002, ApJ, in press (astro-ph/0201104)

de Ruiter H.R. et al., 1997, A&A, 319, 7

Devlin M. et al., 2001, in J. Lowenthal & D.H. Hughes eds., Deep Millimetre Surveys: Implications for Galaxy Formation and Evolution World Scientific, p. 59 (astro-ph/0012327)

Dey A., Graham J.R., Ivison R.J., Smail I., Wright G.S. & Liu M.C., 1999, ApJ, 519, 610.

Downes D., et al., 1999, A&A, 347, 809

Dunlop J.S., 2001, in FIRSED2000, eds. I.M. van Bremmel et al., Elsevier New Astronomy Reviews (astro-ph/0101297).

Dunlop J.S. et al., MNRAS, 2002, submitted

Dunne L., Eales S.A., Edmunds M., Ivison R., Alexander P., & Clements D.L., 2000, MNRAS, 315, 115

Eales S.A., et al., 1999, Ap.J., 515, 518

Eales S.A., et al., 2000, A.J., 120, 2244

Fardal M.A., Katz N., Weinberg D.H., Davé R., Hernquist L., 2002, ApJ, submitted (astro-ph/0107290)

Fox M.J., et al., 2002, MNRAS, 331, 839.

Frayer D.T., et al., 2000, A.J., 120, 1668

Gear W.K., Lilly S. J., Stevens J.A., Clements D.L., Webb T.M., Eales S.A., Dunne, L., 2000, MNRAS, 316, 51.

Helou P. et al. 1985, ApJ, 440, 35

Hughes D.H., Gear W.K., Robson E.I., 1990, MNRAS, 244, 759.

Hughes D.H., Robson E.I., Dunlop J.S., Gear W.K., 1993, MNRAS, 263, 607

Hughes D.H., et al., 1998, Nature, 394, 241

Hughes D.H., et al., 2002, MNRAS, submitted, (*paper I*, astro-ph/0111547)

Hornschemeier A., et al., 2000, Ap.J., 541, 49

Ivison R.I. et al., 1998, MNRAS, 298, 583

Ivison R.J., et al., 2000, MNRAS, 315, 209

Klaas U. et al. 2001. A&A, 379, 823

Lilly S.J., et al., 1999, Ap.J., 518, 441

Lutz D., et al., 2001, A&A, 378, 70.

Richards E.A., et al., 1998, Ap.J., 116, 1039

Richards E.A., 1999, Ap.J., 513, L9

Richards E.A., 2000, Ap.J., 533, 611

Saunders D.B. Rowan-Robinson M., Lawrence A., Efstathiou G., Kaiser N., Ellis R. S., Frenk C. S., 1990, MNRAS, 242, 318

Scott D. et al., 2000, A&A, 357, 5.

Scott S., et al., 2002, MNRAS, 331, 817.

Smail I., et al., 1997, MNRAS, 490, L5

Smail I., et al., 1999, MNRAS, 308, 1061

Smail I., Ivison R.J., Blain A.W., Kneib J.-P., 2002, MNRAS, 331, 495.

Thompson R., et al., 1999, A.J., 117, 17

Webb T.M.A., et al., 2002, ApJ, submitted (astro-ph/0201181).

Williams R.E., et al., 1996, A.J., 112, 1335

Yun M.S. & Carilli C.L., 2002, Ap.J., in press (*YC02*, astro-ph/0112074).

## APPENDIX A: REDSHIFT ESTIMATES FOR INDIVIDUAL SUB-MM GALAXIES

(available at  
<http://www.inaoep.mx/~itziar/papers/dllapp.ps.gz>)